JCTC Journal of Chemical Theory and Computation

Article

pubs.acs.org/JCTC

Can Continuum Thermodynamics Characterize Wenzel Wetting States of Water at the Nanometer Scale?

Frédéric Leroy* and Florian Müller-Plathe

Eduard-Zintl-Institut für Anorganische und Physikalische Chemie and Center of Smart Interfaces, Technische Universität Darmstadt, Petersenstrasse 22, 64287 Darmstadt, Germany

Supporting Information

ABSTRACT: We address the question of how solid−liquid surface free energy is affected by nanometer scale roughness. We proceed through molecular dynamics calculations of the solid−liquid surface free energy of water in a collapsed wetting state on rough nonpolar surfaces characterized by an array of parallel linear grooves. We establish a continuum equation based on Wenzel and Cassie−Baxter approaches to predict the solid−liquid surface free energy variations of systems, where the vertical and horizontal surfaces of the groove have different interactions with water and where the groove geometry can be varied. We show that the molecular simulations results agree with the prediction of the continuum equation under the condition that the groove is wider than three water molecular diameters and deeper than one molecular diameter.

INTRODUCTION

The general framework of the present study is the theoretical understanding of the thermodynamic properties of interfaces between liquids and solid or soft substrates exhibiting roughness at the nanometer scale. There is experimental evidence that substrates with multiple scale roughness that include a pattern at the nanometer scale are likely to generate highly efficient water-repellent materials.[1] Among other examples, the effect of nanoscale roughness was found to play a role in the hydrodynamic properties of solid−liquid interfaces.[2] Nanoscale roughness also is expected to influence the heat-transfer efficiency through the interface between a substrate and a fluid.[3]

Kuna et al. emphasized that although interfaces structured at the nanometer scale are ubiquitous, the way nanostructure influences the surface free energy of these interfaces remain largely unexplored.[4] This is primarily due to the fact that the solid−liquid surface free energy cannot be directly measured by conventional methods, such as droplet contact angle measurements, which are routinely employed to assess the wetting properties of rugged substrates. The contact angle equations of Cassie−Baxter[5] and Wenzel[6] are often used as a quantitative framework to understand these measurements. These equations will be commented on in more details within the Theoretical Basis Section. As for now, it is sufficient to mention that Cassie−Baxter and Wenzel equations were derived on the basis of continuum interfacial thermodynamics. They were intended to predict the contact angles of droplets on rugged surfaces depending on the contact angles on chemically identical but perfectly flat surfaces and on parameters characterizing the heterogeneity patterns. Therefore, they may be used to indirectly relate contact angle measurements to surface free energies, although establishing such relationships may not be a straightforward task.[7,8] Kuna et al. also pointed out that those contact angle equations are continuum equations that may be inadequate to describe interfaces at the molecular scale.[4]

The molecular simulation approach whose typical length scale spans over the range of a few Ångstroms to a few tens of nanometers constitutes a good tool to probe whether continuum contact angle equations can be used to quantify the thermodynamics of nanostructured interfaces. The methodology most often employed is to perform calculations of the contact angles of nanoscopic droplets on well characterized rough and/or chemically heterogeneous surfaces with nanometer or subnanometer sized patterns. Molecular simulation studies generally report that the Cassie−Baxter equation is predictive in most cases at the nanometer scale.[9−11] While other studies found that the applicability of Wenzel's equation at that length scale was more restricted,[11−15] the simulation results qualitatively followed the trend predicted by this equation. Wang et al. recently illustrated that a Cassie−Baxter equation that simultaneously takes into account the effect of molecular scale roughness, and chemical heterogeneity is likely to offer a generalized framework to analyze contact angle simulations on surfaces with roughness at the nanometer scale.[16] Furthermore, it has strongly been suggested in the case of water that magnitude of the surface free energies is established within a distance of a few molecular diameters from the substrate.[17−21] This observation may explain why agreement is often found between macroscopic contact angle equations and the results of test studies at the nanometer scale.

Another approach to address the predictive character of Cassie−Baxter and Wenzel equations at the nanometer scale is to directly compute the surface free energies of the nanorough interfaces instead of contact angles which may significantly depend on the droplets size[22] and/or on the interactions close to the droplet's perimeter.[16] Moreover, the independent knowledge of interfacial free energies is important as the balance between these quantities may predict whether a liquid

Special Issue: Wilfred F. van Gunsteren Festschrift

Received: February 1, 2012
Published: April 23, 2012

forms discrete domains (droplets) on a substrate or spreads and forms a film for which no contact angle is defined.[23] Mittal and Hummer recently used molecular dynamics simulations to compute the surface free energy of water interacting with a surface exhibiting sinusoidal roughness whose periodicity was varied.[17] They observed that the surface free energy was subject to large variations, including change of its sign, under the influence of roughness. Errington and successive co-workers have developed a Monte Carlo methodology to obtain the interfacial thermodynamic properties of a liquid droplet on either a smooth or a rugged surface from an interfacial potential without resorting to the simulation of a droplet.[24,25] These authors have addressed the applicability of Wenzel's contact angle equation at the nanometer scale for Lennard-Jones fluids interacting with nonpolar surfaces.[26] They found that Wenzel's predictions are likely to fail when the roughness periodicity is smaller than 20 molecular diameters. We recently employed and developed thermodynamic integration methods to compute the variations of the solid−liquid surface free energy for smooth and rough interfaces, too.[27−30] We tested the basic idea on which Wenzel constructed his equation in the context of water interacting with a rough model graphite surface including superficial defects.[29] We found that the surface free energy was dominated by the contour length of the defects pattern. Such a result could not be predicted by the formalism of Wenzel. The purpose of the present report is to extend this work and identify other possible deviations to the continuum thermodynamics approach.

To that end, we investigate whether the Wenzel and Cassie−Baxter approaches to describe the surface free energy of collapsed wetting states are still valid on the nanometer scale for substrates which simultaneously exhibit geometrical roughness and chemical heterogeneity. We proceed by computing the solid−liquid surface free energy of water in contact with an infinite array of linear grooves dug in a nonpolar substrate. We formulate a continuum equation that is intended to predict the composite solid−liquid surface free energy variations depending on the roughness parameters and the surface free energies of the smooth and homogeneous surface components. We quantify the effect of combining nanometer scale roughness and chemical heterogeneity on the surface free energy by means of molecular dynamics simulations. We compare the results obtained at the molecular level to the continuum predictions and identify the factors that yield results deviating from the continuum equation. We show that, at least for the particular groove system modeled here, the continuum approach remains valid unless water experiences too strong a confinement due to the narrowness of the groove.

THEORETICAL BASIS

The implementation of roughness on solid substrates yields a variety of wetting states. On the one hand, a sessile liquid droplet on a rugged substrate can be characterized by a fully suspended wetting state due to the presence of air pockets within the roughness pattern underneath the droplet.[31] For high surface tension fluids, such as water, the liquid−air interfaces which thus occur largely contribute to enhance the droplet's free energy and contact angle. On the other hand, in contrast to the possible metastable suspended states, the collapsed wetting states characterized by full contact between the droplet's base and the roughness pattern may be the most stable.[32,33] In addition, numerous intermediate metastable states that cannot simply be designated as being either collapsed or suspended exist. As was mentioned in the introduction, Wenzel[6] and Cassie and Baxter[5] defined theoretical frameworks to predict the contact angle of a liquid droplet on rugged surfaces. Swain and Lipowsky[34] later revisited these approaches to account for gravity and line tension effects as well as the possibility that roughness is combined with chemical heterogeneity. For completeness, it should be mentioned that Israelachvili and Gee proposed a contact angle equation to describe the situation of chemically heterogeneous substrates based on molecular properties, such as the dipole moments.[16,35,36]

Wenzel and Cassie and Baxter considered the so-called Young's contact angle equation as a starting point:

$$\cos\theta = \frac{\gamma_{sv} - \gamma_{sl}}{\gamma_{lv}} \tag{1}$$

In their approach, γ stands for the surface free energies of the solid−vapor (sv), solid−liquid (sl), and liquid−vapor (lv) interfaces. Seeking to quantify the contact angle of a droplet in a collapsed state, Wenzel introduced a roughness factor r to account for the enhancement of the contact surface area between the droplet and the solid, and r is defined as the ratio between the actual solid surface available for solid/liquid contact and the projected area of the solid surface in the plane parallel to it. He recognized that the change in the actual contact surface area induced by roughness yields a change in the interfacial excess free energies of the interfaces between the liquid and the solid and between the vapor and the solid. Wenzel next turned the interfacial excess free energies into surface free energies, i.e., interfacial excess free energies per unit area. Then, he obtained that the difference$\gamma_{sv} - \gamma_{sl}$ on a flat surface is changed into $r(\gamma_{sv} - \gamma_{sl})$ on the rugged surface. Since $r > 1$, Wenzel's result shows that the intrinsic surface free energy properties of a flat surface are likely to be amplified by roughness. He introduced the modified surface free energies in eq 1 to obtain the contact angle θ_W on the rugged surface from its value θ on a perfectly flat surface:

$$\cos\theta_W = r\cos\theta \tag{2}$$

The Cassie−Baxter equation usually employed is intended to quantify the contact angle of a droplet in a suspended wetting state induced by roughness, where water is strictly located atop the roughness pattern. The underlying reasoning to compute the change in contact angle arising from the presence of air−liquid interfaces underneath the droplet is similar to Wenzel's. It is based on quantifying the change in excess interfacial surface free energies per unit area of the interfaces between the liquid and the vapor and the solid. The surface free energy difference $\gamma_{sv} - \gamma_{sl}$ on the flat surface is turned into $f(\gamma_{sv} - \gamma_{sl}) + (1 - f)\gamma_{lv}$ on the rough surface to account for the presence of liquid−air interfaces, and f stands for the fraction of solid surface area available for direct contact between the suspended droplet and the solid. Inserting the previous result into eq 1 yields the so-called Cassie−Baxter contact angle equation. This procedure can be generalized in order to obtain an equation that aims to predict the contact angle of a droplet on a flat surface exhibiting multiple chemical heterogeneity domains. Each heterogeneity domain i accounts for a fraction f_i of the total flat solid surface area. The contact angle on the heterogeneous surface θ_{CB} is obtained as a linear combination of the contributions $\cos\theta_i$ of each heterogeneity domain:

$$\cos\theta_{CB} = \sum_i f_i \cos\theta_i \tag{3}$$

The range of applicability of Wenzel and Cassie–Baxter equations to understand contact angle behaviors has been extensively discussed in the recent years.[7,8,37−41] It is not our aim to further discuss this topic. We are instead interested in assessing whether the surface free energy equations on which they are based also keep their form for interfaces, which are rough at the nanometer scale, and for which molecular details are likely to play a role. Wang et al. addressed this question in the context of chemically heterogeneous surfaces with heterogeneity domains of molecular size through contact angles calculations.[16] Although computed contact angles were found to deviate from the prediction of the original Cassie–Baxter equation (eq 3), these authors found that taking into account surface roughness through solvent accessible surfaces instead of the surface fractions f_i yielded improved agreement between computed and predicted values of the contact angles.

We consider rough surfaces whose roughness is arranged in the form of linear grooves. We study collapsed wetting states where all the interfacial water is in direct contact with the entire available surface. We focus our attention on systems where the vertical and horizontal walls of the grooves have different interactions with water. Such a situation of interaction contrast would be met in a system where a solid surface is covered with a self-assembled monolayer of asymmetric molecules similar to the dialkyl disulfides in the experimental study of Li et al.[42] or the self-assembled monolayers in the simulation work of Acharya et al.[3] These systems exhibit roughness patterns that originate from the inhomogeneous distribution of molecular sizes. Roughness is then characterized by vertical and horizontal surfaces. The interaction of the liquid with the horizontal surfaces would be dominated by the amphiphile's headgroup, while the interaction with the vertical surfaces would be influenced more strongly by the amphiphile's tail. Another example would consist of a solid surface in which grooves are dug such that water molecules interacting with the groove face different crystallographic planes on the horizontal and vertical walls of the surface. The vertical and horizontal walls considered independently yield two different excess interfacial free energies with water. We aim to compute the solid–liquid surface free energy γ_{sl}^{groove} of the water-groove system, depending on the contrast between the free energy contributions of the vertical and horizontal walls. Thus, we introduce $\gamma_{sl,H}$ as the solid–liquid surface free energy of the system defined such that water interacts with an infinitely flat surface identical to the groove's horizontal walls. A similar quantity that characterizes the interaction of water with the vertical walls is $\gamma_{sl,V}$. Let a_H and a_V, respectively, be the total surface area of the horizontal and vertical surfaces with which water is in contact. We consider a unit cell of a groove surface (see Figure 1). The unit cell's cross section is parallel to the (xy) plane, and its projected cross sectional area is $A = L_x \times L_y$. Thus, the unit cell excess surface free energy of a water-groove system is

$$A\gamma_{sl}^{groove} = a_H\gamma_{sl,H} + a_V\gamma_{sl,V} \tag{4}$$

Note that eq 4 was obtained following the reasoning that yields eqs 2 and 3, taking into account the inhomogeneous chemical nature of the roughness pattern. Assume that the groove runs in x direction and that its depth is h. It is straightforward to show

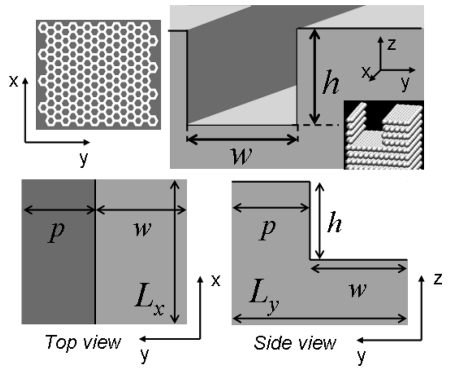

Figure 1. Schematic representations of the groove system. Top left: (0001) graphite surface. Top right: Three-dimensional representation of the groove. Bottom left: Side view in the (yz) plane. Bottom right: Top view in the (xz) plane. Definitions of the groove's geometric parameters: p is the protrusion's width, w is the groove's width, h is the groove's depth, and L_x and L_y are the x and y simulation cell lengths in the x and y direction, respectively.

that $a_H = L_x \times L_y$ and $a_V = 2L_x \times h$. Inserting these relationships in eq 4 leads to

$$\gamma_{sl}^{groove} = \gamma_{sl,H} + \frac{2h}{L_y}\gamma_{sl,V} \tag{5}$$

We now transform eq 5 so that it formally describes the composite surface free energy of systems including both roughness and chemical heterogeneity. The form of the desired equation depends on parameters related to these features:

$$\gamma_{sl}^{groove} = r_H f_H \gamma_{sl,H} + r_V f_V \gamma_{sl,V} \tag{6}$$

where r_H and r_V stand for the roughness factor of the groove's horizontal and vertical wall components, respectively. They are both defined according to Wenzel as the ratio between the true area of the surfaces with which water is in direct contact and the unit cell cross sectional area. Therefore,

$$r_H = r_V = \frac{2h + L_y}{L_y} \tag{7}$$

f_V is the ratio between the area of the vertical walls and the area of the surface accessible to water, while f_H is the ratio between the area of the horizontal walls and the area of the surface accessible to water. It is straightforward to obtain for f_H and f_V:

$$f_H = \frac{L_y}{2h + L_y} \tag{8}$$

and

$$f_V = \frac{2h}{2h + L_y} \tag{9}$$

One obtains $r_H f_H = 1$ by combining the results above. Thus, the composite surface free energy equation (eq 6) simplifies to

$$\gamma_{sl}^{groove} = \gamma_{sl,H} + r_V f_V \gamma_{sl,V} \tag{10}$$

Note that although this equation was derived for the geometry of the groove system, its analytical form remains identical for any system where the total area of the horizontal surfaces is equal to the unit cell cross sectional area.

Equation 10 can be written in a form where the composite surface free energy depends on the surface free energy of the

system with a flat homogeneous surface $\gamma_{sl,H}$, an heterogeneity factor $\alpha = r_V f_V$ that accounts for the surface's heterogeneity in chemistry and topography and a contrast factor $c = \gamma_{sl,V}/\gamma_{sl,H}$ that quantifies the difference in the intrinsic thermodynamic excess properties of the horizontal and vertical surfaces:

$$\gamma_{sl}^{groove} = \gamma_{sl,H}(1 + c\alpha) \quad (11)$$

Although eq 11 is given as a general equation to compute γ_{sl}^{groove} depending on the relevant parameters that characterize heterogeneous groove surfaces, we will focus in the present work on probing the validity of eq 11 with a single value of the contrast factor c. In the present case $c = -1.9$. Note that this value is specific to the material we employed in the present study. The procedure that yields eq 6 can be repeated to treat the solid–vapor surface free energies of the rough surfaces and combined with the results dealing with the solid–liquid surface free energies to obtain a generalized Cassie–Baxter–Wenzel contact angle equation, as was noted by Wang et al.[16]

COMPUTATIONAL DETAILS

In order to probe the validity of eq 10 in the framework of nanometer scale rough surfaces, we performed molecular dynamics simulations of water in interaction with rough solid surfaces whose reference is the flat (0001) graphite surface (see Figure 1). We used graphite as our example because its layered structure yields a locally anisotropic distribution of carbon atoms. As can be seen in Figure 1, the solid surface was oriented such that the carbon layers were parallel to the (xy) plane of the simulation cell. The water phase extended in the z direction. The top and bottom surfaces of the groove, called horizontal walls, are aligned parallel to the (xy) plane. The vertical walls are the surfaces oriented parallel to the (xz) plane. Thus, the external field experienced by water in the vicinity of the surface differs depending on which crystallographic plane it is in contact with; the number of carbons per area is larger for the interface formed by a graphite sheet (xy plane, 38.2 carbon atoms/nm^2) than by the interface formed by the side of a stack of graphite sheets (xz plane, 13.8 carbon atoms/nm^2). The density difference conveniently mimics the general situation where roughness is associated with chemical heterogeneity. Moreover, dealing with solid surfaces with clear roughness patterns permits precise determination of the vertical and horizontal components contributions and facilitates the formal treatment.

Roughness was implemented by switching off the interaction between water and some selected carbon atoms. We did not explicitly remove carbon atoms from the simulation cell in order to avoid surface reconstruction during the simulations. In real systems, the removal of atoms would probably result in a reconstruction of the surface due to a major perturbation of graphite's electronic structure. Our goal is to draw qualitative and quantitative conclusions that we expect to be valid in the general framework of water interacting with solid surfaces simultaneously exhibiting roughness and chemical heterogeneity. It is also important to note that the interaction between water and the vertical walls (parallel to the xz plane) as well as the horizontal wall (parallel to the xy plane) of the groove are of the same nature. In fact, we did not introduce electrostatic charges to compensate the virtual breaking of chemical bonds due to the roughness implementation. Although the results presented here should be interpreted in the framework of model systems where the surface is a nonpolar substrate, it will be shown that the difference in solid–liquid surface free energy between the vertical and horizontal walls is approximately as large as 50% of the surface tension of water.

Calculations were performed with a surface having one linear groove. Although the simulation domain was finite, the groove appeared infinitely long to water because periodic boundary conditions were used parallel to the interfaces (i.e., parallel to the xy plane). Because of these periodic boundary conditions, water behaved as if it were interacting with an infinite array of parallel grooves. Note that periodic boundary conditions were also implemented perpendicular to them (i.e., along the z direction). The width of the groove w, its length L_x, and its depth h as well as the width of the protrusion $p = L_y - w$ are schematically defined in Figure 1. These geometric parameters were varied so as to sample several values of the heterogeneity factor $r_V f_V$. The values of $r_V f_V$ are reported in Table 1 and were computed according to the definitions in eqs 7 and 9. The heterogeneity factor is independent of the groove's width because the total horizontal area is also the simulation cell cross sectional area. It must be mentioned that we considered atoms as points to compute the different geometric quantities listed above. In other words, we did not include excluded volume considerations in defining the geometry. This is consistent with the continuum view we adopted to derive eqs 10 and 11 where atomic volumes were neglected.

Table 1. Groove's Geometric Parameters and Solid–Liquid Surface Free Energies γ_{sl}[a]

	h (nm)	L_y (nm)	w (nm)	p (nm)	$r_V f_V$	γ_{sl} (mJ/m^2)
A	0	2.95	0	0	0	−12.49 ± 0.61
	0.34	2.95	1.60	1.35	0.230	−4.64 ± 0.60
	0.68	2.95	1.60	1.35	0.461	−0.84 ± 0.66
	1.04	2.95	1.60	1.35	0.691	5.51 ± 1.54
	1.36	2.95	1.60	1.35	0.922	9.77 ± 1.68
	1.70	2.95	1.60	1.35	1.152	15.34 ± 1.98
B	1.36	3.69	2.34	1.35	0.737	5.99 ± 1.50
	1.36	4.43	3.08	1.35	0.614	2.66 ± 1.32
	1.36	5.17	3.82	1.35	0.527	−1.00 ± 1.16
C	1.36	2.95	2.33	0.62	0.922	9.97 ± 1.80
	1.36	2.95	1.23	1.72	0.922	13.66 ± 1.70
D	–	3.06	–	–	–	23.92 ± 0.62

[a] h stands for the depth, w is the width, $r_V f_V$ is the heterogeneity factor. L_y is simulation cell dimension along the y direction. The value of the simulation cell's length in the x direction, L_x, was identical in all simulations and amounted to 3.408 nm. All simulations whose value of L_y was 2.951 nm contained 2790 water molecules. The simulations where L_y was 3.689, 4.427, and 5.165 nm contained 3348, 3906, and 4185 water molecules, respectively.

We performed free energy calculations at normal conditions (298 K, 101.3 kPa) by means of molecular dynamics simulations using a thermodynamic integration scheme called the phantom-wall method.[27] The calculations carried out in this context yield the difference in surface free energy of the solid–liquid interface between the actual surface and a reference surface whose surface free energy with water is the liquid–vapor surface free energy.[29] We define the solid–liquid surface free energy as the solid–liquid interfacial excess Gibbs free energy per cross-sectional area of the simulation cell. The liquid–vapor surface tension of the water model used here is 59.5 mJ/m^2. This was determined in a previous study.[29] The method has already been applied in computations dealing with

water in interaction with graphite model surfaces.[29] Further technical details about the phantom-wall method are extensively described elsewhere.[27,28] Water was modeled using the rigid three sites SPC/E model.[43] The Lennard-Jones distance and energy parameters are σ_O = 0.3166 nm and ε_O = 0.6502 kJ/mol, respectively, while the electrostatic charges are q_O = −0.8476 and q_H = +0.4238 e. Note that there is no Lennard-Jones parameter for hydrogen in this model. The interactions between the water molecules and graphite were modeled by means of Lennard-Jones pair interactions between oxygen and carbon with the parameters optimized by Werder et al., i.e., σ_{CO} = 0.319 nm and ε_{CO} = 0.392 kJ/mol.[22] The internal dynamics of graphite was modeled according to the work of Bedrov and Smith.[44] The number of water molecules and the number of carbon atoms in the simulation cells were varied depending on the solid surface size. These details are reported in the caption of Table 1.

It is important to note that simulations were always initiated with a configuration in which water molecules were placed on a cubic lattice that was above the top carbon layers of the surfaces. After equilibration, the system spontaneously relaxed into a collapsed wetting state when the groove depth was at most 1.02 nm, which is three times the distance between two carbon layers. When the depth was larger, the system was trapped in a suspended wetting state. In order to drive the system to a collapsed state, we increased the strength of the interaction between water and a two-atom thick layer along the vertical walls. In the case where the depth was 1.7 nm (5 times the interlayer distance), we also had to increase the interaction parameter between water and the carbon atoms of the groove's horizontal ground layer to ε_{CO} = 0.627 kJ/mol so as to prepare the collapsed state. We performed the phantom-wall free energy calculations with the modified interactions described above. Therefore, the obtained surface free energy was not the target one which concerns systems where only carbon atoms of identical type are present. We carried out an additional free energy calculation to determine the difference in surface free energy between the system where water is in a collapsed state on a modified grooved surface and the target system where water is a collapsed state on a grooved surface with identical carbon atoms (standard thermodynamic integration without the phantom wall procedure). To preserve the clarity of the manuscript, we describe the procedure outlined above in detail in the Supporting Information.

RESULTS

We report the variations of γ_{sl}^{groove} with respect to the heterogeneity factor $r_V f_V$ in Table 1. These values were obtained by varying the depth of the groove h (data set A in Table 1) or the width of the cavity w (data set B in Table 1) or the width of the protrusion p (data set C in Table 1). The variations are also plotted in Figure 2. In addition, the plot includes the value of γ_{sl}^{groove} of the interface between water and smooth graphite (diamond symbol). This value is $\gamma_{sl,H}$ according to our nomenclature. It can be observed that γ_{sl}^{groove} increases with h when w and p are kept constant (filled black circle symbols in Figure 2), that γ_{sl}^{groove} also increases when w decreases, while h and p are maintained at fixed values (empty square symbols in Figure 2), and that γ_{sl}^{groove} also is larger than the smooth interface free energy, when either w or p are varied while h and $r_V f_V$ are constant. The common feature of the results described above is that the graphite's smooth surface ($r_V f_V$ = 0) has the lowest surface free energy with water.

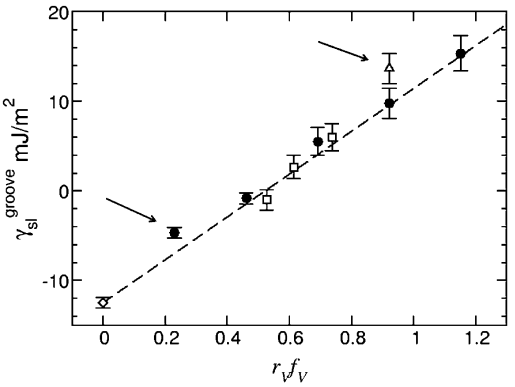

Figure 2. Variations of the solid−liquid surface free energy of the groove−water systems γ_{sl}^{groove} with respect to the heterogeneity factor $r_V f_V$. The diamond is the result characterizing the flat surface. The filled black circles refer to the simulations where the groove's depth was varied, while other geometric parameters were kept constant. The empty squares are the results of the simulations where the groove's width was varied, while other geometric parameters were maintained constant. The white triangle represents the value of γ_{sl}^{groove} for the narrowest groove's width. The dashed line represents the prediction of eq 10. The arrows point out the main deviations to the prediction of eq 10.

Roughness implemented in either way increases the surface free energy above that of smooth graphite−water systems, that is to say, the solid surface increases its nonwettable character when its roughness increases. It must also be observed that γ_{sl}^{groove} changes its sign under the influence of the roughness parameter. The results reported above are in apparent contradiction with the work of Wenzel, which shows that the magnitude of the solid−liquid surface free energy should be amplified by roughness. Because of the negative value of $\gamma_{sl,H}$ in the present case, the rough graphite should have a lower surface free energy with water than the smooth graphite if the result obtained by Wenzel applied. However, his reasoning did not include the possibility that chemical heterogeneity adds to roughness, i.e., the vertical and horizontal walls of the groove can in fact have different interactions with water. In the present case, the contrast in interaction energy arises from the fact that water faces different crystallographic planes when it is in the vicinity of the horizontal and vertical walls. Note that significant differences in surface free energy induced by the interaction with different crystallographic planes of a given material have been characterized by Grzelak and Errington in a molecular simulation study on pure Lennard-Jones systems.[45]

In order to show that the variation of γ_{sl}^{groove} with respect to either the groove depth or the width can be captured by eq 10, we computed the surface free energy $\gamma_{sl,V}$ of the interface between water and an infinitely flat surface where the graphite's carbon layers are oriented perpendicular to the interface. This configuration is similar to the one encountered when water faces the groove's vertical walls. The independent determination of $\gamma_{sl,V}$ led to a value of 23.9 ± 0.6 mJ/m^2 (reported as the data set D in Table 1). Equipped with both $\gamma_{sl,H}$ and $\gamma_{sl,V}$, we plotted the variation of γ_{sl}^{groove} with respect to $r_V f_V$ given by eq 10 as the dotted line in Figure 2, so as to compare the obtained trend with the simulation results. Only two disagreements between the computed and predicted data occur (pointed out in Figure 2). A first deviation from the prediction of eq 10 arises when the groove's depth is 0.34 nm at $r_V f_V$ = 0.230. A second deviation arises when the groove width is 1.23 nm at

$r_V f_V$ = 0.922. Possible explanations for these deviations will be discussed later in the text. For the remaining situations, it can be said that the agreement between the computed and predicted values shown in Figure 2 is excellent. This quantitative agreement indicates that the predictions of eq 10 are valid despite the relatively high level of confinement experienced by water for grooves of width of less than 10 nm. We should recall that eq 10 was derived on the basis of a continuum thermodynamic description according to which fine variations in molecular details are ignored.

In order to further understand the results outlined above, we first focus on the set where only the groove depth was varied (data set A in Table 1, squares in Figure 2). We report in Figure 3 the spatial distribution of the average interaction potential

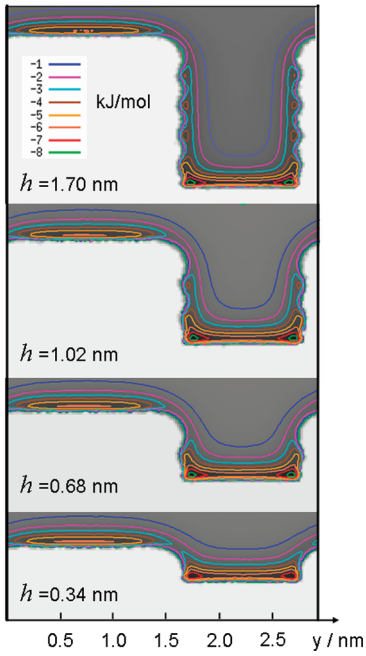

Figure 3. Average interaction potential energy between individual water molecules and graphite. Each plot was obtained at a given value of the groove's depth, while the groove's width was maintained constant. The color scale in the top-plot given in kJ/mol applies to all plots.

energy between individual water molecules and the carbon atoms computed from the simulations. The plot was obtained by assigning water molecules to volume elements of 0.025 × 0.025 × 0.025 nm^3 and averaging over time and space along the direction parallel to the groove. We present the isosurface plots of the interaction energy normalized per water molecule obtained for the systems where the groove depth was 1.7, 1.04, 0.68, and 0.34 nm. The interaction potential energy is negative when water molecules are either located close to the horizontal surfaces or close to the vertical surfaces. For all systems, the top of the protrusion and the bottom of the groove are energetically not exactly equivalent, although the interaction energy at the center of both these locations is identical (approximately −6 kJ/mol). It must also be observed that the strongest interaction potential energy of water with the vertical surfaces of the groove is weaker than it is with the horizontal surfaces (approximately −3.5 and −6 kJ/mol, respectively). In all cases, the line along the x direction (i.e., parallel to the groove) at the bottom corner of the groove represents an energy minimum of the water−carbon interaction. Nevertheless, this minimum is not very deep when compared with the minimum occurring at the center of the horizontal surfaces (approximately −8 and −6 kJ/mol, respectively). Note that the bottom corner interaction energy is increased by approximately 1 kJ/mol in the case of h = 0.34 nm. The top corner of the groove is a maximum of the water−carbon potential energy landscape. The locations on the vertical and horizontal axis of the −3 kJ/mol isosurface boundaries are unchanged when the groove is deeper than 0.68 nm (cyan curves in Figure 3). This suggests that the intrinsic interaction features of the horizontal and vertical walls with water are established once the groove reaches a depth of 0.68 nm. The variation of γ_{sl}^{groove} observed in Figure 2 (black squares) shows that the vertical walls energetic characteristics are increased linearly when the groove's depth becomes larger.

We report in Figure 4 the average spatial distribution of the water mass density in the groove system. The data were

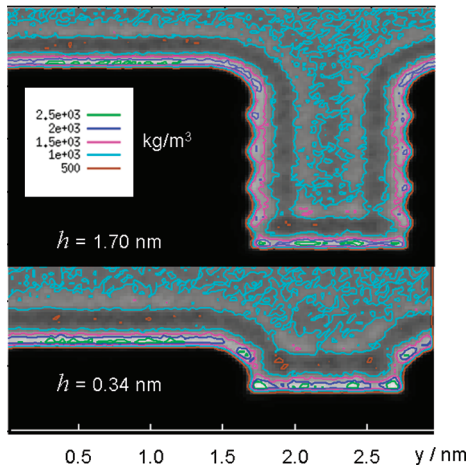

Figure 4. Average water mass-density distribution obtained in the cases where h = 1.7 and 0.34 nm (top and bottom, respectively). The color scale is given in kg/m^3 and applies to both plots. The gray shades represent locations where low water mass density is observed (approximately lower than water bulk mass density).

obtained by means of the same averaging procedure described above. The system's behavior with respect to two values of the depth is illustrated, i.e., h = 1.7 and 0.34 nm. The behavior observed for intermediate values of h is comparable to the case of h = 1.7 nm and is thus not shown here. The result is consistent with what was already found for the water−carbon interaction energy distribution. A water layering structure is evident in both plots where an excess of water is found on the horizontal protrusion surface and on the ground surface of the groove. For grooves deeper than 0.34 nm, the layered structure also exists along the vertical surfaces of the groove. However, the average water mass density within these layers is markedly different for vertical and horizontal surfaces. It is of the order of 2500 kg/m^3 close to the horizontal surfaces, while it is approximately 1650 kg/m^3 close to the vertical surfaces. This is again consistent with the observation we made concerning the water−carbon energy distribution. Although the average water mass-density distribution within the deepest groove is centered on water's bulk value, it is shown in Figure 4 that water actually organizes itself in four layers parallel to the vertical surfaces. There are two layers whose mass density is approximately 1650 kg/m^3 in the immediate vicinity of the surface, and two other layers whose mass density is approximately 1200 kg/m^3 on

dx.doi.org/10.1021/ct300089j | J. Chem. Theory Comput. 2012, 8, 3724−3732

both sides of the central plane of the groove. This four-layer structure is observed once the groove's depth is at least 0.68 nm. Such an ordering in the system may be responsible for decreasing the entropy, and it would therefore possibly contribute to increase the surface free energy. It is also important to note that the excess of water found at the top corner when h = 0.34 nm is larger than it is for deeper grooves. Therefore, more water molecules have to experience the energetically unfavorable top corner location which yields an unfavorable contribution to the surface free energy in all cases. This contribution reaches its strongest intensity in the case where h = 0.34 nm.

Pal et al. reported studies on the effect of roughness on the hydrophobic surfaces of *n*-eicosane and perfluoro-*n*-eicosane.[30,46,47] The solid−liquid surface free energy of water with the related flat materials is expected to be in the range of 25−30 mJ/m^2 based on values of the contact angle of water of the order of 120° or less.[48] This value can be compared with what we obtained for the surface free energy of the interfaces between water and the vertical walls. Those authors implemented a groove having a depth of 0.5 nm and a width of 1 nm in *n*-eicosane. In contrast to our results, they did not report excess of water either in or at the bottom corner of the groove.[46] They also did not observe an excess of water at the bottom circumference of holes having a diameter of 2.5 nm and a depth of 0.5 nm in *n*-eicosane and perfluoro-*n*-eicosane.[30,47] However, a slight excess of water was found at the center of these cavities. Although a slight excess of water was found on the top horizontal surfaces of *n*-eicosane and perfluoro-*n*-eicosane, no excess was found either on the bottom surface or parallel to the vertical surfaces. It is interesting to note that although the vertical walls of graphite have a positive surface free energy with water, excess of water is observed close to the vertical walls. This is explained by the fact that the distance between two carbon layers in graphite is approximately the size of a water molecule. Therefore, these interlayer positions represent adsorption sites for water, though weak in comparison with the bottom corners of the groove.

In order to explain why excess of water molecules can be found at the top corner of the graphite groove, we examined the spatial average number of hydrogen bonds per water molecule distribution within the groove. The hydrogen bonds were defined by means of an energetic criterion following Jorgensen et al.[49] We employed this criterion in our previous contribution on the effect of superficial nanometer scale roughness on solid−liquid surface free energies of water−graphite interfaces.[29] A plot of this distribution in the case of h = 1.7 nm can be found in Figure S1 of the Supporting Information. All other systems exhibit comparable features. It was found that the average number of hydrogen bonds per water molecule is close to its bulk value in the vicinity of the top corner of the groove, while it is decreased in the vicinity of the bottom corner. In contrast, the perturbation of the hydrogen-bonds network parallel to the vertical surfaces of the groove is not much different from what it is parallel to the top horizontal surface or parallel to the bottom of the groove. The number of hydrogen bonds per water molecule within the groove reaches a value identical to the bulk value of the model. The number of hydrogen bonds per water molecules at the top corner, as described above, explains why excess of water is found at this location: Water preserves its hydrogen-bonding network despite the local unfavorable interaction with the surface.

We summarize the information obtained from the spatial distributions of interaction potential energy, mass density, and hydrogen bonds to draw the following picture: Water has lower interaction potential energy with the surface at the bottom corner of the groove than on the horizontal and vertical surfaces, while this interaction energy is higher at the top corner than on the horizontal and vertical surfaces. Although the bottom corner position yields a favorable enthalpy contribution to the excess free energy in comparison to the flat surface, the top corner position leads instead to an unfavorable enthalpy contribution. It is expected that the imbalance between both contributions has a weak magnitude for simple geometric reasons. This imbalance is constant for grooves that are deep enough, so that a water molecule at one corner does not feel the influence of the other corner. When the groove depth increases, water is exposed to a larger area of vertical walls, which causes the free energy to increase. This is due to the unfavorable enthalpy contribution that originates from the lower water−carbon attraction by the vertical walls. Water within the groove is organized in layers with a weaker intensity than on the horizontal surfaces, though. Layering may cause an unfavorable entropy contribution to the surface free energy. Gain and loss of enthalpy are contributed in connection with the hydrogen-bonds network perturbation at the top and bottom corners, respectively. The agreement between the simulation results and the prediction of the continuum equation indicates that the major contribution that drives the variation of the surface free energy with respect to the groove's depth is the contrast in interaction energy between the vertical and horizontal walls with water. If there is an imbalance between the corner contributions of opposite sign mentioned above, it is negligible in comparison to the changes induced by the presence of the vertical walls. The result that the molecular dynamics simulations calculations are consistent with the continuum picture is somehow astonishing because the groove's width is of the order of 1 nm. One would expect such a reduced dimension to yield peculiar effects due to confinement. In the case of pure Lennard-Jones systems, Grezlak and Errington reported deviations from Wenzel's equation when the roughness periodicity was shorter than 20 atom diameters.[26] Although the value they report is larger than our finding by approximately a factor of 2−3, the roughness pattern they used was different and did not include an energetic contrast between the different components of the surface as large as in our work. These authors also pointed out that the nature of the interactions within the system may play a significant role. It remains to be investigated whether long-range interactions between the fluid and the substrate yield a different behavior. This is outside the scope of the present work and should be addressed in a future contribution.

Still in the present context of solid−liquid short-range interactions, a deviation from the continuum thermodynamics approach has been observed at low groove depth ($r_V f_V$ = 0.230). We have shown in our previous contribution that the surface free energy of water−graphite surfaces exhibiting superficial defects depends on the defects contour length per unit area. The groove having the smallest depth is such a superficial defect. Therefore, the surface free energy with water is driven by the extent of the perturbation in one dimension along the groove (x axis in the present case). In contrast, two-dimension considerations are required to quantify the surface free energy of deeper grooves. In other words, the surface free energy of the groove with the smallest depth is dominated by

the top corner high energy, while the vertical wall energy dominates the other water-groove systems. Nevertheless, the deviation to the prediction of eq 10 is approximately 3 mJ/m^2, which is only a small fraction of the surface tension of water.

We now examine the data set B (Table 1) of γ_{sl}^{groove} values, which were obtained by varying the groove's width while its depth was maintained at 1.36 nm and while the protrusion width was kept constant, too. The results are the squares that appear in Figure 2. It can be observed that γ_{sl}^{groove} decreases when the width of the groove increases. This is quantitatively consistent with the prediction of eq 10. Indeed, increasing the width increases the total horizontal area with its favorable contribution to the surface free energy. Another effect of increasing the groove's width is to lower the confining effect of a narrow groove. If a strong entropy decrease existed in connection with this effect at w = 1.60 nm, it should be lowered as the groove's width is enhanced. Our results do not, however, support a strong contribution of this effect because one does not observe any major deviation to the prediction of eq 10 while increasing w. Note that eq 10 does not account for such an entropy effect.

Data set C was produced in an attempt to violate the predictive behavior of eq 10 by narrowing the width of either the groove or the protrusion, while the heterogeneity factor $r_V f_V$ was kept constant. The protrusion was made so thin that water molecules on each side of it can interact with each other through it. This massive reduction of p to 0.62 nm did not yield a deviation from the prediction of eq 10 (Table 1). Note that the effective size of the protrusion increases to a value of approximately 0.94 nm if the carbon atoms excluded volumes are taken into account. This value is still shorter than the cutoff of 1.375 nm that was employed to compute the pair interactions. In contrast, reducing the groove's width to 1.23 nm yields a value of γ_{sl}^{groove} that significantly deviates from the prediction of eq 10 (see the triangle symbol in Figure 2). The value of γ_{sl}^{groove} exceeds the analytical prediction by approximately 4 mJ/m^2. Narrowing the groove has consequences, though weak in magnitude, on the water−graphite interaction energy distribution and on the water mass-density distribution within the groove (Figure 5). The main features observed in wider grooves are conserved (see Figures 3 and 4 for comparison.) The main change in the interaction energy distribution concerns the extent of the region where water molecules experience interaction energies higher than −1 kJ/mol. Due to increased confinement, this region has a lower volume in the case of the narrowest groove, while regions where the interaction is lower than −2 kJ/mol are unaffected. This can presumably be attributed to the short-range nature of the interactions between water and the surface. The effect of confinement on the mass density shows three excess regions parallel to the groove's vertical walls. This reveals that water forms three vertical layers within the groove. The distribution of hydrogen bonds per water molecule is similar to what was obtained for the wider grooves. Although the mass-density distribution of water indicates that there is a slightly higher level of ordering within the groove, the hydrogen-bond network is insensitive to the reduction of space (see Figures S1 and S2 in the Supporting Information). The increased level of ordering mentioned above may be responsible for the central layer in a three-layer system to have a higher energy or lower entropy than the two central layers in a four-layer system, yielding the observed deviation to the prediction of eq 10. Alternatively, one may invoke the possibility that the width of the narrower groove is not commensurate with the thickness of three water layers. Such an effect has been evidenced in studies of confined fluids.[50] Precise understanding of these effects is beyond the scope of the present work.

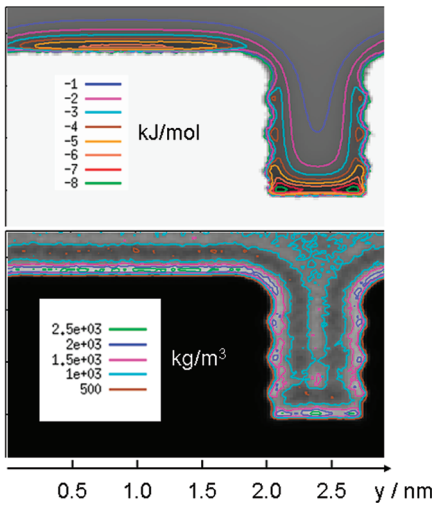

Figure 5. Top: Average interaction energy distribution between water molecules considered individually and graphite for the system whose groove width was 1.23 nm. Bottom: Water mass-density distribution of the same system.

CONCLUSIONS

We considered interfacial systems where water was in contact with rough solid surfaces in collapsed wetting states. The roughness pattern was arranged in the form of linear grooves whose vertical and horizontal walls had interactions of different strength with water, which yielded chemical heterogeneity. We derived a continuum equation based on the additivity of surface contributions to predict the solid−liquid surface free energy of the water-groove systems depending on the surface free energies of the horizontal and vertical interfaces and the roughness parameters. The equation shows that two main degrees of freedom can be employed to tune the surface free energy of a collapsed state, namely the groove's geometric parameters and the contrast between the chemical nature of the horizontal and vertical walls of the groove. The established equation suggests that the stability of the collapsed and the suspended states can be inverted depending on how the groove's geometric features and chemical contrast are chosen.

We performed molecular dynamics computations of the solid−liquid surface free energies of systems of water interacting with graphite-based model surfaces containing linear grooves. The horizontal and vertical surfaces had different intrinsic surface free energies and the roughness had characteristic dimensions of only a few nanometers. We showed that the continuum equation described the molecular dynamics results for most of these systems. Deviations from the continuum model occurred only either when the width of the groove became of the order of 1 nm or when the groove was one atom diameter deep. However, even for these cases, the magnitude of the deviations was only a few percent of the surface tension of water.

Note that we have probed the validity of a continuum thermodynamics equation down to a few nanometers only in the framework of (a) a nonpolar surface material, (b) a relatively high chemical contrast between the vertical and

horizontal walls, and (c) for groove geometries. For the sake of generality, it remains to establish whether these conclusions apply to substrates exhibiting other topographies and/or electrostatic fluid−substrate interactions.

■ ASSOCIATED CONTENT

Supporting Information

Description of the material, surface free energy computations for groove's depths larger than 1.02 nm, and average number of hydrogen bonds per water molecule spatial distributions. This material is available free of charge via the Internet at http://pubs.acs.org.

■ AUTHOR INFORMATION

Corresponding Author

*E-mail: f.leroy@theo.chemie.tu-darmstadt.de

Notes

The authors declare no competing financial interest.

■ ACKNOWLEDGMENTS

F.M.-P. thanks Prof. van Gunsteren, his group, and the Botherington-Smythe-Holdsworth society for encouragement and support at a decisive stage of his career. This work was financially supported by the Deutsche Forschungsgemeinschaft (DFG) and the Center of Smart Interfaces (CSI) of the TU Darmstadt. We are grateful to the high performance computing center of the TU Darmstadt for allocating computation time and to the John von Neumann Institute for Computing in Jülich for allocating computation time on the machine JUROPA. We thank Claudia Schwartzkopff for inspiring discussions.

■ DEDICATION

We dedicate this article to Wilfred van Gunsteren on the occasion of his 65th birthday.

■ REFERENCES

(1) Kwon, Y.; Patankar, N.; Choi, J.; Lee, J. *Langmuir* **2009**, *25*, 6129−6136.
(2) Joly, L.; Ybert, C.; Bocquet, L. *Phys. Rev. Lett.* **2006**, *96*, 046101.
(3) Acharya, H.; Mozdziert, N. J.; Keblinski, P.; Garde, S. *Ind. Eng. Chem. Res.* **2011**, *51*, 1767−1773.
(4) Kuna, J. J.; Voïtchovsky, K.; Singh, C.; Jiang, H.; Mwenifumbo, S.; Ghorai, P. K.; Stevens, M. M.; Glotzer, S. C.; Stellacci, F. *Nat. Mater.* **2009**, *8*, 837−842.
(5) Cassie, A. B. D.; Baxter, S. *Trans. Faraday Soc.* **1944**, *40*, 546−551.
(6) Wenzel, R. N. *Ind. Eng. Chem.* **1936**, *28*, 988−994.
(7) Gao, L. C.; McCarthy, T. J. *Langmuir* **2009**, *25*, 7249−7255.
(8) Milne, A. J. B.; Amirfazli, A. *Adv. Coll. Interf. Sci.* **2012**, *170*, 48−55.
(9) Lundgren, M.; Allan, N. L.; Cosgrove, T.; George, N. *Langmuir* **2003**, *19*, 7127−7129.
(10) Lundgren, M.; Allan, N. L.; Cosgrove, T. *Langmuir* **2007**, *23*, 1187−1194.
(11) Daub, C. D.; Wang, J. H.; Kudesia, S.; Bratko, D.; Luzar, A. *Faraday Disc.* **2010**, *146*, 67−77.
(12) Yang, C.; Tartaglino, U.; Persson, B. N. J. *Eur. Phys. J. E: Soft Matter Biol. Phys.* **2008**, *25*, 139−152.
(13) Yong, X.; Zhang, L. T. *Langmuir* **2009**, *25*, 5045−5053.
(14) Hirvi, J. T.; Pakkanen, T. A. *Langmuir* **2007**, *23*, 7724−7729.
(15) Hirvi, J. T.; Pakkanen, T. A. *J. Phys. Chem. B* **2007**, *111*, 3336−3341.
(16) Wang, J. H.; Bratko, D.; Luzar, A. *Proc. Natl. Acad. Sci.U.S.A.* **2011**, *108*, 6374−6379.
(17) Mittal, J.; Hummer, G. *Faraday Disc.* **2010**, *146*, 341−352.
(18) Lee, C. Y.; McCammon, J. A.; Rossky, P. J. *J. Chem. Phys.* **1984**, *80*, 4448−4455.
(19) Hua, L.; Zangi, R.; Berne, B. J. *J. Phys. Chem. C* **2009**, *113*, 5244−5253.
(20) Janecek, J.; Netz, R. R. *Langmuir* **2007**, *23*, 8417−8429.
(21) Patel, H. A.; Nauman, E. B.; Garde, S. *J. Chem. Phys.* **2003**, *119*, 9199−9206.
(22) Werder, T.; Walther, J. H.; Jaffe, R. L.; Halicioglu, T.; Koumoutsakos, P. *J. Phys. Chem. B* **2003**, *107*, 1345−1352.
(23) de Gennes, P.-G.; Brochart-Wyart, F.; Quéré, D. *Capillarity and Wetting Phenomena. Drops, Bubbles, Pearls, Waves*. Springer Science: New York, 2004; pp 16−18.
(24) Grzelak, E. M.; Errington, J. R. *J. Chem. Phys.* **2008**, *128*, 014710.
(25) Kumar, V.; Sridhar, S.; Errington, J. R. *J. Chem. Phys.* **2011**, *135*, 184702.
(26) Grzelak, E. M.; Errington, J. R. *Langmuir* **2010**, *26*, 13297−13304.
(27) Leroy, F.; dos Santos, D. J. V. A.; Müller-Plathe, F. *Macromol. Rapid Commun.* **2009**, *30*, 864−870.
(28) Leroy, F.; Müller-Plathe, F. *J. Chem. Phys.* **2010**, *133*, 044110.
(29) Leroy, F.; Müller-Plathe, F. *Langmuir* **2011**, *27*, 637−645.
(30) Pal, S.; Roccatano, D.; Weiss, H.; Keller, H.; Müller-Plathe, F. *ChemPhysChem* **2005**, *6*, 1641−1649.
(31) Tuteja, A.; Choi, W.; Ma, M. L.; Mabry, J. M.; Mazzella, S. A.; Rutledge, G. C.; McKinley, G. H.; Cohen, R. E. *Science* **2007**, *318*, 1618−1622.
(32) Bocquet, L.; Lauga, E. *Nat. Mater.* **2011**, *10*, 334−337.
(33) Callies, M.; Quéré, D. *Soft Matter* **2005**, *1*, 55−61.
(34) Swain, P. S.; Lipowsky, R. *Langmuir* **1998**, *14*, 6772−6780.
(35) Israelachvili, J. N.; Gee, M. L. *Langmuir* **1989**, *5*, 288−289.
(36) Halverson, J. D.; Maldarelli, C.; Couzis, A.; Koplik, J. *Soft Matter* **2010**, *6*, 1297−1307.
(37) Gao, L. C.; McCarthy, T. J. *Langmuir* **2007**, *23*, 3762−3765.
(38) Marmur, A.; Bittoun, E. *Langmuir* **2009**, *25*, 1277−1281.
(39) McHale, G. *Langmuir* **2007**, *23*, 8200−8205.
(40) Nosonovsky, M. *Langmuir* **2007**, *23*, 9919−9920.
(41) Bormashenko, E. *Langmuir* **2009**, *25*, 10451−10454.
(42) Li, G. F.; Flores, S. M.; Vavilala, C.; Schmittel, M.; Graf, K. *Langmuir* **2009**, *25*, 13438−13447.
(43) Berendsen, H. J. C.; Grigera, J. R.; Straatsma, T. P. *J. Phys. Chem.* **1987**, *91*, 6269−6271.
(44) Bedrov, D.; Smith, G. *Langmuir* **2006**, *22*, 6189−6194.
(45) Grzelak, E. M.; Shen, V. K.; Errington, J. R. *Langmuir* **2010**, *26*, 8274−8281.
(46) Pal, S.; Weiss, H.; Keller, H.; Müller-Plathe, F. *Langmuir* **2005**, *21*, 3699−3709.
(47) Pal, S.; Weiss, H.; Keller, H.; Müller-Plathe, F. *Phys. Chem. Chem. Phys.* **2005**, *7*, 3191−3196.
(48) Nishino, T.; Meguro, M.; Nakamae, K.; Matsushita, M.; Ueda, Y. *Langmuir* **1999**, *15*, 4321−4323.
(49) Jorgensen, W. L.; Chandrasekhar, J.; Madura, J. D.; Impey, R. W.; Klein, M. L. *J. Chem. Phys.* **1983**, *79*, 926−935.
(50) Eslami, H.; Mozaffari, F.; Moghadasi, J.; Müller-Plathe, F. *J. Chem. Phys.* **2008**, *129*, 194702.